AIChE

Support-Dependent Activity of Noble Metal Substituted Oxide Catalysts for the Water Gas Shift Reaction

Parag A. Deshpande and Giridhar Madras
Dept. of Chemical Engineering, Indian Institute of Science, Bangalore 560012, India

DOI 10.1002/aic.12177
Published online January 20, 2010 in Wiley Online Library (wileyonlinelibrary.com).

The water gas shift reaction was carried out over noble metal ion substituted nanocrystalline oxide catalysts with different supports. Spectroscopic studies of the catalysts before and after the reaction showed different surface phenomena occurring over the catalysts. Reaction mechanisms were proposed based upon the surface processes and intermediates formed. The dual site mechanism utilizing the oxide ion vacancies for water dissociation and metal ions for CO adsorption was proposed to describe the kinetics of the reaction over the reducible oxides like CeO_2. A mechanism based on the interaction of adsorbed CO and the hydroxyl group was proposed for the reaction over ZrO_2. A hybrid mechanism based on oxide ion vacancies and surface hydroxyl groups was proposed for the reaction over TiO_2. The deactivation of the catalysts was also found to be support dependent. Kinetic models for both activation and deactivation were proposed. © 2010 American Institute of Chemical Engineers *AIChE J,* 56: 2662–2676, 2010
Keywords: water gas shift reaction, supported catalysis, ionic substitution, deactivation, modeling

Introduction

The conventionally used catalysts for the water gas shift reaction (WGS) consist of ternary solutions of Cu/ZnO/Al_2O_3.[1–6] The catalysts suffer from the problems of pyrophoricity and require special methods for preparation and handling.[7] With the requirement of high purity hydrogen for fuel cell applications, newer and novel catalysts are required for catalyzing WGS. The use of noble metals has been reported for catalyzing WGS.[8] A good dispersion of the noble metal is required to make effective use of the metal. This can be achieved by the use of an inert solid as the support and dispersion of the noble metal as the active species. For WGS and the CO oxidation reaction, Al_2O_3 and SiO_2 are used as supports.[9–11] The choice of these supports is based on the cost, inertness, and stability of the material.

Correspondence concerning this article should be addressed to G. Madras at giridhar@chemeng.iisc.ernet.in.

WGS involves oxidation of CO to CO_2 and a corresponding reduction of H_2O to H_2. For such redox reactions, a catalyst with metal-support interactions is expected to enhance the activity by inducing redox couples, which facilitate the overall catalysis cycle. Therefore, it is of interest to study the kinetics of the reaction over the various supports and observe the influence of the various supports on the kinetics of the reaction. It is important to note that not only the active species, but also the support and their combination, play a crucial role.

A number of supports have been reported for catalyzing WGS using different noble metals. The supports mainly included Al_2O_3, CeO_2, ZrO_2, TiO_2, and the mixed oxides with high dispersion of Pt, Pd, and Au.[12–20] Various surface reactions taking place over the catalyst are influenced by the identity of the support. Azzam et al.[21,22] have reported the influence of the support on the path followed for WGS reaction over the Pt metal catalysts with various supports. The difference in the reducibility of the support was found to be responsible for the stabilization of the various intermediate species and, hence, different pathways were described during the reaction over the catalysts.

Table 1. Precursor Requirements and Structure of Solids Synthesized by Solution Combustion

S. No	Compound	Precursors and Stoichiometry (molar)	Crystal Structure	Crystallite Size (nm)	Ref.
1	CeO_2	CAN + ODH = 1:2.4	Cubic (Fluorite)	38	29
2	$Ce_{0.99}Pd_{0.01}O_{2-\delta}$	CAN + PdCl + ODH = 0.99:0.01:2.4	Cubic (Fluorite)	49	29
3	$Ce_{0.99}Pt_{0.01}O_{2-\delta}$	CAN + PtN + ODH = 0.99:0.01:2.4	Cubic (Fluorite)	49	29
4	$Ce_{0.98}Pd_{0.02}O_{2-\delta}$	CAN + PdCl + ODH = 0.98:0.02:2.4	Cubic (Fluorite)	54	29
5	$Ce_{0.98}Pt_{0.02}O_{2-\delta}$	CAN + PtN + ODH = 0.98:0.02:2.4	Cubic (Fluorite)	49	29
6	$Ce_{0.85}Zr_{0.15}O_{2-\delta}$	CAN + ZN + ODH = 0.85:0.15:2.4	Cubic (Fluorite)	51	23
7	$Ce_{0.83}Zr_{0.15}Pd_{0.02}O_{2-\delta}$	CAN + ZN + PdCl + ODH = 0.83:0.15:0.02:2.4	Cubic (Fluorite)	25	23
8	$Ce_{0.83}Zr_{0.15}Pt_{0.02}O_{2-\delta}$	CAN + ZN + PtN + ODH = 0.83:0.15:0.02:2.4	Cubic (Fluorite)	25	23
9	$Ce_{0.85}Ti_{0.15}O_{2-\delta}$	CAN + TiN + ODH = 0.85:0.15:2.4	Cubic (Fluorite)	36	
10	$Ce_{0.83}Ti_{0.15}Pd_{0.02}O_{2-\delta}$	CAN + TiN + PdCl + ODH = 0.83:0.15:0.02:2.4	Cubic (Fluorite)	31	
11	$Ce_{0.83}Ti_{0.15}Pt_{0.02}O_{2-\delta}$	CAN + TiN + PtN + ODH = 0.83:0.15:0.02:2.4	Cubic (Fluorite)	32	
12	ZrO_2	ZN + ODH = 1:1.96	Tetragonal	31	23
13	$Zr_{0.98}Pd_{0.02}O_2$	ZN + PdCl + ODH = 0.98:0.02:1.96	Tetragonal	31	23
14	$Zr_{0.98}Pt_{0.02}O_2$	ZN + PN + ODH = 0.98:0.02:1.96	Tetragonal	42	23
15	TiO_2	TiN + Gly = 1:1.11	Tetragonal (Anatase)	14	
16	$Ti_{0.98}Pd_{0.02}O_{2-\delta}$	TiN + PdCl + Gly = 0.98:0.02:1.11	Tetragonal (Anatase)	15	
17	$Ti_{0.99}Pt_{0.01}O_{2-\delta}$	TiN + PtN + Gly = 0.99:0.01:1.11	Tetragonal (Anatase)	12	

CAN, ceric ammonium nitrate ($(NH_4)_zCe(NO_3)_6$); PdCl, palladium chloride ($PdCl_2$); ODH, oxalyldihydrazide ($C_2H_6N_2O_4$); ZN, zirconium nitrate ($Zr(NO_3)_4{\cdot}5H_2O$); PtN, tetraammine platinum nitrate ($(NH_3)_4Pt(NO_3)_2$); Gly, glycine ($C_2H_5NO_2$); TiN, titanyl nitrate ($TiO(NO_3)_2$).

The catalysts synthesized in this study have the metals substituted in the crystal lattice in ionic state. The presence of a metal in ionic state induces redox couples in the active species as well as in the support. Metal-support interactions can be observed in systems in which the support is reducible and the metal can exhibit a variable valence state. The differential oxidation and reduction of the metal and the support result in the transfer of the electrons to the reactant species resulting in enhanced redox reactions. Therefore, the reducibility of the support has an influence over the rates of reaction. In our previous studies, we have found the difference in the behavior of Zr modified CeO_2 and ZrO_2 supported ionic catalysts for WGS.[23] From X-ray photoelectron spectroscopy, it was found that in case of reducible supports like CeO_2, the redox couples established between the metal and the support maintain the metal in ionic state. ZrO_2 has a very poor reducibility. Therefore, the ionically substituted metal was found to get reduced to zero state under the reducing conditions of the WGS. Therefore, different pathways can be expected over the supports with different reducibility. According to Bakhmutsky et al.,[24] the highest rates for WGS can be obtained with an optimum reducibility of the support and the thermodynamic properties must be considered for selection of the supports. Therefore, it becomes important to describe the kinetics of the reaction on the basis of the support.

Apart from the high activity, the life of the catalysts is also an important parameter for rendering them suitable for practical applications. Though many WGS catalysts have also been tested for CO oxidation and preferential oxidation reactions, the catalysts have been reported to show significantly different deactivation behavior for the different reactions. Dang and Flytzani-Stephanopoulos[25] have found Pt/CeO_2 and Au/CeO_2 systems to be highly resistant towards deactivation for preferential CO oxidation (PrOx) but is rapidly deactivated under WGS conditions.[26] Therefore, the nature of the catalyst as well as the reaction conditions play an important role in determining the rate of deactivation. In one of our previous studies, we have reported the time variation of the CO concentration during the WGS under daily startup–shutdown conditions.[27] The conversion of CO decreased for La-substituted catalyst even after maintaining exactly identical conditions throughout the course of the reaction. Spectroscopic studies revealed the formation of surface carbonate resulting in a decrease in the activity of the catalyst with reaction time.

The current study aimed at modeling the influence of support on the activity and deactivation of the ionic nanocrystalline oxide catalysts for WGS. Support-dependent models were proposed for describing the kinetics of the WGS. Different surface phenomena were observed over the different supports. The spectroscopic evidences were used in determining the possible surface processes and rate mechanisms were proposed based on elementary pathways. The rate coefficients were derived by non-linear regression.

Experimental

Catalyst synthesis and characterization

All the catalysts were synthesized by solution combustion technique. The technique involves the combustion of a salt of the support, a salt of a noble metal, and a fuel in appropriate molar ratio in solution to yield a highly porous mass of solid. The compounds hence formed have crystallites in nanometer range.[28] Table 1 summarizes the chemical requirements and the stoichiometry required for the synthesis of various compounds. A detailed account of the synthesis can be found elsewhere.[23,27,29]

All the compounds were characterized by powder X-ray diffraction (XRD) and X-ray photoelectron spectroscopy (XPS). XRD were recorded on Philips X'pert diffractometer with CuKα radiations. XPS of the compounds were recorded on Thermo Fisher Scientific Multilab 2000 (England) instrument with AlKα radiations (1486.8 eV). Further details can be found elsewhere.[23,27,29]

Catalytic activity tests

All the reactions were carried out in 4 mm ID quartz tube reactors with the catalysts packed in the form of granules

between ceramic wool. The reactor was heated from outside using an electric furnace. The temperature of the reactor was controlled using a PID controller. The gases were supplied through flow controllers and water was supplied continuously using an HPLC pump (515 model, Waters). The unreacted water was condensed after the reaction and the dry gases were sent for analysis in an online gas-chromatograph (Nano HP-I, Mayura Analyticals, Bangalore, India) in which separation was achieved by a combination of Haye-sep-A and molecular sieve columns. A detailed description of the experimental procedures can be found in our previous work.[29]

Results and Discussion

Structural studies

Powder XRD pattern of all the catalysts was recorded. CeO_2-based catalysts were found to crystallize in fluorite structure. The solid solutions of CeO_2-ZrO_2 and CeO_2-TiO_2 also crystallized in fluorite structure. No peaks corresponding to tetragonal or monoclinic phases of ZrO_2 were observed in the XRD of CeO_2-ZrO_2 solid solutions. Similarly, no lines of rutile or anatase phases of TiO_2 were observed in CeO_2-TiO_2 solid solutions. This showed the formation of single phase solid solutions those can be represented by the formula $Ce_{1-x-y}M_xN_yO_{2-\delta}$, where M represents the noble metal (Pd or Pt) and N represents Zr or Ti. The quantity x represents atom % substitution of noble metal and y represents atom % substitution of Zr or Ti in the support. Typically in our studies, $x = 0.02$ and $y = 0.15$. The peak corresponding to metal was absent showing substitution of the metal in lattice. Noble metal substituted ZrO_2 catalysts crystallized in tetragonal structure. The phase was confirmed by FT-Raman studies. TiO_2 compounds were found to crystallize in anatase phase. The crystallite size of all the compounds was in nanometer range. Table 1 summarizes the important structural deductions obtained by XRD.

XPS of all the elements present in the catalysts were recorded. Ce, Zr, and Ti in all the catalysts were found to be in +4 state. In solid solutions, Zr and Ti were in +4 state. The noble metals were found in ionic state. Pd in all the compounds was in +2 state. Pt was in a mixed oxidation state in all the compounds. The majority of Pt was substituted in +2 state. A very small amount was present as metallic Pt, the rest being in +4 state. In substituted CeO_2 and TiO_2 compounds, the noble metals retained their ionic state after the reaction.[23,27] In substituted ZrO_2 compounds, Pt ions were observed to get reduced to metallic state after the reaction.[23] The XRD patterns and XPS spectra of all the compounds before and after the reaction can be found in our previous works.[23,27,29]

Modeling the WGS reaction over different supports

Dual Site Mechanism. From the XPS of the noble metals before and after the reaction, it is clear that in all the CeO_2-based catalysts, the metal remains in the ionic state during the reaction.[23,27] CeO_2 is a reducible oxide. Therefore, due to its oxygen storage capacity, CeO_2 is liable to release oxygen from the lattice at high temperatures. Substitution of a noble metal in +2 state in Ce^{4+} sites results in the formation of oxide ion vacancies for electrostatic neutrality. We have reported WGS over Pd and Pt ion substituted CeO_2 and found that the kinetics of the reaction can be described by a dual site mechanism.[29] The mechanism essentially considers the adsorption of CO over the metal ion and the dissociation of H_2O over the oxide ion vacancy, giving H_2 and an intermediate oxygen species. The surface reaction between the adsorbed CO and the intermediate oxygen species results in the release of CO_2. To account for the reversibility of the reaction, the reverse reaction counterparts were proposed. Experiments were also carried out to find the rate limiting step. The surface reaction was found to be the rate limiting step. A competitive adsorption of CO and H_2 was proposed to occur over the metal ion and competitive dissociative adsorption of H_2O and CO_2 was proposed to take place over the oxide ion vacancies. Dissociative adsorption of H_2O and CO_2 resulted in the release of H_2 and CO while the surface reactions between the adsorbed species resulted in release of CO_2 and H_2O. Substitution of Zr and Ti is beneficial as the bulk substitution of these elements results in an enhanced oxygen storage capacity[30,31] and, hence, enhanced redox couples are expected.

The various surface reactions can be written as:

$$CO + S_M \Leftrightarrow CO_M \tag{1a}$$

$$H_2O + \text{“v”} \rightarrow \text{“o”} + H_2 \tag{1b}$$

$$CO_M + \text{“o”} \rightarrow CO_2 + \text{“v”} + S_M \tag{1c}$$

$$H_2 + S_M \Leftrightarrow H_{2_M} \tag{1d}$$

$$CO_2 + \text{“v”} \rightarrow \text{“o”} + CO \tag{1e}$$

$$H_{2_M} + \text{“o”} \rightarrow H_2O + \text{“v”} + S_M \tag{1f}$$

Equations 1a and 1d show the reversible adsorption of CO and H_2 over the metal ion, respectively. The oxide ion vacancies formed in the support due to the substitution and reducibility of the support, act as sites for the adsorption of H_2O and CO_2. They appear in Eqs. 1b and 1e as ''v''. The dissociative adsorption of H_2O and CO_2 over the oxide ion vacancies is shown by Eqs. 1b and 1e, respectively, giving the intermediate oxygen species retained on the support. The surface reactions given by Eqs. 1c and 1f result in the release of the product and the relative rates of the two reactions give the effective rate of reaction.

In the above reaction scheme, Eqs. 1d and 1f can be written as separate steps as follows:

$$H_2 + S_M \rightarrow H_{2M} \tag{1g}$$

$$H_{2M} \rightarrow H + H \tag{1h}$$

$$H + H + \text{“o”} \rightarrow H_2O + 2S + \text{“v”} \tag{1i}$$

The dissociation of H_2 over the metal takes place. This may result in the spillover of H to the adjacent vacant site. However, it has been shown, for ionic Pt in CeO_2, that more than one H atom can be stabilized over a single Pt ion.[32] Therefore, step (1h) in the above equation takes place over a single site and, hence, the above set of equations can be

lumped into a single equation (Eq. 1f) without affecting the kinetics of the reaction.

In the above mechanism, the formation of oxide ion vacancies is possible only if the substituted metal is present in +2 state. Although pure CeO_2 also has some oxide ion vacancies, the activity of this catalyst is negligible without substitution. The adsorption of the gases increase on substitution of a metal ion as the metal ions act as centers for adsorption. Further, impregnation of metal does not result in creation of oxide ion vacancies. Therefore, the above mechanism is applicable only when the metal is substituted in ionic form in Ce^{4+} sites with an oxidation state other than +4.

The reaction over unsubstituted CeO_2 can be written as:

$$Ce^{4+}O_2^{2-} + \delta CO \rightarrow Ce_{2\delta}^{3+}Ce_{1-2\delta}^{4+}O_{2-\delta}^{2-} + \delta CO_2 \quad (2a)$$

$$Ce_{2\delta}^{3+}Ce_{1-2\delta}^{4+}O_{2-\delta}^{2-} + \delta H_2O \rightarrow Ce^{4+}O_2^{2-} + \delta H_2 \quad (2b)$$

$$2Ce^{4+}O_2^{2-} + \delta H_2 \rightarrow Ce_{2\delta}^{3+}Ce_{1-2\delta}^{4+}O_{2-\delta}^{2-} + \delta H_2O \quad (2c)$$

$$Ce_{2\delta}^{3+}Ce_{1-2\delta}^{4+}O_{2-\delta}^{2-} + \delta CO_2 \rightarrow Ce^{4+}O_2^{2-} + \delta CO \quad (2d)$$

where δ denotes the oxygen storage capacity of the compound. In the as-synthesized catalyst, Ce is present in +4 state. A partial reduction of Ce^{4+} in CeO_2 takes place in the reducing atmosphere of CO and H_2 and a part of Ce^{4+} goes to Ce^{3+}, shown by Eqs. 2a and 2c. The abstraction of oxygen from the lattice results in the oxidation of CO to CO_2 and the oxygen occupancy of the support decreases by δ. All these processes result in the formation of the reduced catalyst. The catalyst gets oxidized in the oxidizing environment provided by H_2O and CO_2, as shown in Eqs. 2b and 2d. However, in the absence of a strong adsorbent of CO and H_2, the rate of reaction is extremely slow. The substitution of a metal ion results in the formation of sites for adsorption. Moreover, the aliovalent substitution results in the creation of oxide ion vacancies, where the dissociation of the reactants takes place fastening the redox processes given by Eqs. 2a–2d. The pathway for the reaction over noble metal substituted compounds can be given as:

$$Ce_{1-x}^{4+}M_x^{2+}O_{2-x}^{2-} + xCO \rightarrow Ce_{1-x}^{4+}M_x^{0}O_{2-2x}^{2-} + xCO_2 \quad (3a)$$

$$Ce_{1-x}^{4+}M_x^{2+}O_{2-x}^{2-} + xCO \rightarrow Ce_{2x}^{3+}Ce_{1-3x}^{4+}M_x^{2+}O_{2-2x}^{2-} + xCO_2 \quad (3b)$$

$$Ce_{1-x}^{4+}M_x^{0}O_{2-2x}^{2-} + xH_2O \rightarrow Ce_{1-x}^{4+}M_x^{2+}O_{2-2x}^{2-} + xH_2 \quad (3c)$$

$$Ce_{2x}^{3+}Ce_{1-3x}^{4+}M_x^{2+}O_{2-2x}^{2-} + xH_2O \rightarrow Ce_{1-x}^{4+}M_x^{2+}O_{2-x}^{2-} + xH_2 \quad (3d)$$

$$Ce_{1-x}^{4+}M_x^{2+}O_{2-x}^{2-} + xH_2 \rightarrow Ce_{1-x}^{4+}M_x^{0}O_{2-2x}^{2-} + xH_2O \quad (3e)$$

$$Ce_{1-x}^{4+}M_x^{2+}O_{2-x}^{2-} + xH_2 \rightarrow Ce_{2x}^{3+}Ce_{1-3x}^{4+}M_x^{2+}O_{2-2x}^{2-} + xH_2 \quad (3f)$$

$$Ce_{1-x}^{4+}M_x^{0}O_{2-2x}^{2-} + xCO_2 \rightarrow Ce_{1-x}^{4+}M_x^{2+}O_{2-2x}^{2-} + xCO_2 \quad (3g)$$

$$Ce_{2x}^{3+}Ce_{1-3x}^{4+}M_x^{2+}O_{2-2x}^{2-} + xCO_2 \rightarrow Ce_{1-x}^{4+}M_x^{2+}O_{2-2x}^{2-} + xCO_2 \quad (3h)$$

where M represents the substituted noble metal (Pd or Pt) and x represents the atom % substitution. These metal–ion interactions have also been shown experimentally with the help of cyclic voltametry and XPS.[33]

For bulk substitution of metals in the support, the above equations get modified as:

$$Ce_{1-x-y}^{4+}M_x^{2+}N_y^{4+}O_{2-x}^{2-} + xCO \rightarrow Ce_{1-x-y}^{4+}M_x^{0}N_y^{4+}O_{2-2x}^{2-} + xCO_2 \quad (4a)$$

$$Ce_{1-x-y}^{4+}M_x^{0}N_y^{4+}O_{2-2x}^{2-} + xH_2O \rightarrow Ce_{1-x-y}^{4+}M_x^{2+}N_y^{4+}O_{2-x}^{2-} + xH_2 \quad (4b)$$

$$Ce_{1-x-y}^{4+}M_x^{2+}N_y^{4+}O_{2-x}^{2-} + xH_2 \rightarrow Ce_{1-x-y}^{4+}M_x^{0}N_y^{4+}O_{2-2x}^{2-} + xH_2O \quad (4c)$$

$$Ce_{1-x-y}^{4+}M_x^{0}N_y^{4+}O_{2-2x}^{2-} + xCO_2 \rightarrow Ce_{1-x-y}^{4+}M_x^{2+}N_y^{4+}O_{2-2x}^{2-} + xCO_2 \quad (4d)$$

where N represents the metal substituted in bulk (Zr or Ti) and y represents the atom % substitution. Clearly, from all of the above equations, in the presence of reducing agents like CO and H_2, reduction of the metal occurs. Oxidation of metal by corresponding reduction of the support is shown by Eq. 3c. These metal-support interactions have been observed using XPS studies[33] and we have also observed the same in our case. Partial reduction of the support was observed in the XPS after the reaction. Therefore, equilibrium occurs between the oxidized and reduced states of the metal and the support and the following equations can be written for the metal-support interaction.

$$Ce_{1-x}^{4+}M_x^{0}O_{2-2x}^{2-} \leftrightarrow Ce_{2x}^{3+}Ce_{1-3x}^{4+}M_x^{2+}O_{2-2x}^{2-} \quad (5)$$

The above set of interactions show the changes in the oxidation state of the metal and ionic metal gets reduced to metallic state during the reaction cycle. However, due to high ionic dispersion and reaction temperatures, the cluster formation does not take place and the dispersion of the metal is maintained. Pierre et al.[34] have shown that for ceria-based Pt catalysts, Pt^{2+} state can be observed and the catalyst showed high activity due to ionic nature. The dispersion was maintained and the metal retained ionic state due to the thermal processes. Apart from the Pt^0/Pt^{2+} cycle, Pt^{2+}/Pt^{4+} cycle can also exist resulting in the creation of more oxide ion vacancies. However, this cycle can be present in presence of a strong oxidizing agent like oxygen, which can fully oxidize Pt. In WGS, where H_2O acts as an oxidizing agent, this cycle is assumed not to occur.

The metal oxidation–reduction cycle is possible only if the support is reducible. Therefore, the mechanism following the elementary steps given by Eqs. 1a–1f was used to describe the kinetics of the reaction over CeO_2-based catalysts. We obtained the following rate expression by solving the elementary reaction rate expressions for Eqs. 1a–1f.

$$r = \frac{\{K_1k_3[CO](1+K_4[H_2]) - K_4k_6[H_2](1+K_1[CO])\}(k_2[H_2O]+k_5[CO_2])}{(1+K_1[CO])(1+K_4[H_2])(k_2[H_2O]+k_5[CO_2]) + (1+K_4[H_2])K_1k_3[CO] + (1+K_1[CO])K_4k_6[H_2]} \quad (6)$$

The details of the derivation and the underlying assumptions are given in Appendix A.

Surface Hydroxyl Mechanism. We propose this mechanism to describe the kinetics of the reaction over ZrO_2-based catalysts. Zr^{4+} in ZrO_2 is a highly acidic site. Moreover, the reducibility of ZrO_2 is very less. Therefore, under the WGS conditions, the metal which was initially substituted in ionic form, gets reduced to the metallic state according to the following equations:

$$Zr^{4+}_{1-x}M^{2+}_{x}O^{2-}_{2-x} + xCO \rightarrow Zr^{4+}_{1-x}M^{0}_{x}O^{2-}_{2-2x} + xCO_2 \quad (7a)$$

$$Zr^{4+}_{1-x}M^{2+}_{x}O^{2-}_{2-x} + xH_2 \rightarrow Zr^{4+}_{1-x}M^{0}_{x}O^{2-}_{2-2x} + xH_2O \quad (7b)$$

Equations 7a and 7b are analogous to Eqs. 3a and 3e in which the reduction of the metal ion to metallic state takes place. Because of the reducible nature of CeO_2, Eqs. 3b and 3f follow. But due to the non-reducibility of ZrO_2, the reactions are limited to those given by Eqs. 7a and 7b and the interactions given by Eq. 5 are absent. As a result, further oxidation of the metal to ionic state does not take place. Over a period of time, all of the ionic metal reduces to zero state. This has been observed in the spectra of the Pt4f in $Zr_{0.98}Pt_{0.02}O_2$.[23] Therefore, the phenomena over ZrO_2-based catalyst is essentially those involving adsorption of CO and H_2 over noble metals and surface reactions.

The acidic Zr^{4+} sites act as adsorption sites for H_2O. This results in the formation of surface hydroxyl groups. The surface hydroxyl groups on ZrO_2 are well reported and their presence has been confirmed by infrared spectroscopy.[35–37] We have also found an increase in O1s peak intensity after the reaction around 532 eV corresponding to the oxygen in hydroxyl group.[23] This showed the formation of surface hydroxyl group during the reaction. Therefore, the dissociation of H_2O over ZrO_2 support to give hydroxyl intermediate can be expected. The mechanism can be given as follows:

$$CO + S_M \Leftrightarrow CO_M \quad (8a)$$

$$H_2O + ZrO_2 \rightarrow H_2ZrO_3 \quad (8b)$$

$$H_2ZrO_3 + CO_M \rightarrow CO_2 + H_2 + ZrO_2 + S_M \quad (8c)$$

$$H_2 + S_M \Leftrightarrow H_{2_M} \quad (8d)$$

$$CO_2 + ZrO_2 \rightarrow ZrO_3^{2-} + CO \quad (8e)$$

$$H_{2_M} + ZrO_3^{2-} \rightarrow H_2ZrO_3 + S_M \quad (8f)$$

$$H_2ZrO_3 \rightarrow H_2O + ZrO_2 \quad (8g)$$

The XPS of Zr before and after the reaction shows Zr in +4 state. The above mechanism is consistent with this observation. In all the above steps, +4 state of Zr was maintained. The surface processes taking place following the above mechanism can be represented by the following equations:

$$CO + S_M \Leftrightarrow CO_M \quad (9a)$$

$$H_2O + S_{Zr} \rightarrow S_{Zr}\cdot O + H_2 \quad (9b)$$

$$CO_M + S_{Zr}\cdot O \rightarrow CO_2 + S_{Zr} + S_M \quad (9c)$$

$$H_2 + S_M \Leftrightarrow H_{2_M} \quad (9d)$$

$$CO_2 + S_{Zr} \rightarrow S_{Zr}\cdot O + CO \quad (9e)$$

$$S_{Zr}\cdot O + H_{2_M} \rightarrow H_2O + S_{Zr} + S_M \quad (9f)$$

The rate of reaction for the above sequence is given as:

$$r = \frac{(k_{31}K_{29}[CO] - k_{34}K_{32}[H_2])(k_{30}[H_2O] + k_{33}[CO_2])}{k_{31}K_{29}[CO] - k_{34}K_{32}[H_2] + (1 + K_{29}[CO] + K_{32}[H_2])(k_{30}[H_2O] + k_{33}[CO_2])} \quad (10)$$

A more elementary set of surface processes can be written as follows:

$$CO + S_M \Leftrightarrow CO_M \quad (11a)$$

$$H_2O + S_{Zr} \Leftrightarrow H_2O_{Zr} \quad (11b)$$

$$S_{Zr} + H_2O_{Zr} \rightarrow OH_{Zr} + H_{Zr} \quad (11c)$$

$$OH_{Zr} + S_{Zr} \rightarrow O_{Zr} + H_{Zr} \quad (11d)$$

$$O_{Zr} + CO_M \rightarrow CO_{2_{Zr}} + S_M \quad (11e)$$

$$CO_{2_{Zr}} \Leftrightarrow CO_2 + S_{Zr} \quad (11f)$$

$$H_{Zr} + H_{Zr} \rightarrow H_2 + 2S_{Zr} \quad (11g)$$

$$H_2 + S_M \Leftrightarrow H_{2_M} \quad (11h)$$

$$CO_2 + S_{Zr} \Leftrightarrow CO_{2_{Zr}} \quad (11i)$$

$$CO_{2_{Zr}} + S_{Zr} \rightarrow CO_{Zr} + O_{Zr} \quad (11j)$$

$$CO_{Zr} \rightarrow CO + S_{Zr} \quad (11k)$$

$$H_{2_M} + O_{Zr} \rightarrow H_2O_{Zr} + S_M \quad (11l)$$

$$H_2O_{Zr} \Leftrightarrow H_2O + S_{Zr} \quad (11m)$$

According to the above set of equations, the adsorption of CO takes place over the metal, given by Eq. 11a. Similarly, H_2O can be adsorbed over the acidic Zr^{4+} sites reversibly. This is shown by Eq. 11b. S_M and S_{Zr} represent the vacant metal and Zr site for adsorption, respectively. The interaction of the adsorbed H_2O with the adjacent vacant Zr site can result in the splitting of H_2O and spillover of H to the adjacent site to give intermediate OH and H species on Zr. Similarly, the interaction of OH with another vacant Zr site can give intermediate O and H species. These steps are shown by Eqs. 11c and 11d. The intermediate O species can react with the adsorbed CO to give CO_2 adsorbed over the Zr site by spillover and the metal site becomes free. The desorption of CO_2 from Zr site releases CO_2. The H species formed in the steps 11c and 11d can interact to release hydrogen and make the Zr sites free. The formation of H_{Zr} species over ZrO_2 supports has been reported and it

is proposed that reverse spillover of H takes place during the decomposition of the intermediates.[38]

To account for the reverse reaction, the adsorption of H_2 over the metal and CO_2 over Zr sites is proposed. The dissociation of CO_2 over Zr results in the release of CO and creates an intermediate O species, given by Eq. 11j. Interaction of this O species with the adsorbed H_2 yields H_2O. In this manner, Eqs. 11a–11m account for all the surface phenomena occurring over ZrO_2-based catalysts.

The reaction scheme presented by the above set of equations differs from that proposed for CeO_2-based solutions in the utilization of lattice oxygen. In CeO_2-based solid solutions, lattice oxygen utilization occurs resulting in reduced ceria, which in turn gets oxidized by the utilization of oxygen from the reactants. However, in ZrO_2-based catalysts, reduction and lattice oxygen utilization does not take place. Rather, dissociation of water over Zr sites takes place, which results in the formation of an adsorbed oxygen species. The difference between the adsorbed O species and "o" in case of CeO_2 catalysts is that the latter is adsorbed on oxide ion vacancies, which can be found in low index planes while the adsorption sites for O species over ZrO_2 are low coordination sites.[39] Therefore, this mechanism can also be considered as a type of redox mechanism. Depending upon the surface structure and the reducibility of the catalyst, a particular intermediate is formed. Graf et al.[40] have observed the difference in the function of mono and multi-coordinated monoclinic Pt/ZrO_2 for WGS. Mono-coordinated sites were found to be responsible for intermediate formation whereas multi-coordinated sites were found to be responsible for intermediate decomposition. A similar approach is followed in the proposed reaction scheme, where the dissociation of intermediates is due to the interaction with the adjacent sites.

The complete reaction sequence given by Eqs. 11a–11m can be reduced to those given by Eqs. 9a–9f by lumping some of the steps. In CO and CO_2 rich environment, the hydroxyl groups immediately interact to give surface formate species, which decomposes to give an intermediate oxygen species over Zr^{4+} ions. These steps have been shown by lumping of all the intermediate steps into Eqs. 9b and 9e. Baiker and coworkers[41–44] have studied in detail the hydrogenation of CO_2 over the various metal-ZrO_2 catalysts. One of the steps in such reactions is the reverse WGS. Formate decomposition to give CO has been reported using vibrational spectroscopy over Au/ZrO_2 catalysts.[43] The release of H_2 by decomposition of surface hydroxyl yielding CO_3^{2-} has been shown by FTIR studies.[42] Further decomposition of CO_3^{2-} to give CO_2 and intermediate oxygen species is accounted in the above reaction mechanism by surface interactions of adsorbed CO and CO_2 over the support given by Eqs. 9c and 9e. Monte Carlo studies have also shown the presence of intermediate oxygen species.[45] Surface oxygen removal was found to be energetically difficult and, hence, kinetically slow and rate controlling process. Therefore, reactions 9a through 9f represent a complete set of the surface processes taking place over ZrO_2 supported noble metals.

Hybrid Mechanism. This mechanism is proposed for describing the WGS activity of noble metal substituted TiO_2. The reducibility of TiO_2 is lesser than that of CeO_2.[46] However, the exchange of lattice oxygen is indeed possible. This has been proved for WGS using oxygen isotope exchange technique.[47] Therefore, the dual site mechanism proposed for CeO_2-based compounds can be applied in this case also. Kondarides and coworkers[19,47–49] have investigated WGS over noble metal impregnated TiO_2. Their studies using SSITKA-DRIFTS and isotopic exchange strongly favor the redox mechanism involving the utilization of lattice oxygen. Several other investigators have explained WGS activity using the redox mechanism in which the lattice oxygen is utilized for the oxidation of CO to CO_2. The splitting of H_2O over the oxide ion vacancy reoxidizes the support. The scanning tunneling microscopy and density functional theory calculations have shown the dissociation centers for H_2O in rutile TiO_2 to be the oxide ion vacancies.[50] Similar results were obtained by Brookes et al. for TiO_2 (110) surface.[51] Combustion synthesized TiO_2 crystallizes in anatase phase. Under the WGS conditions, formation of small quantities of rutile phase takes place.[27] Therefore, the redox mechanism can be expected to occur over TiO_2 supported compounds. However, an equally well reported mechanism over TiO_2 catalysts is the associative route in which the reaction proceeds via the utilization of surface hydroxyl groups.[51–53] Azzam et al.[21,22] have carried out pulse experiments on TiO_2-based catalysts and have found the requirement of surface hydroxyl groups for the reaction to proceed. TGA studies on combustion synthesized TiO_2 have shown large concentration of surface hydroxyl groups.[54]

Therefore, to describe WGS over combustion synthesized TiO_2, it becomes important to consider the presence of the surface hydroxyl groups. There have been arguments of the presence of both redox as well as associative mechanisms for WGS over TiO_2.[21] Therefore, to describe the activity of TiO_2-based compounds, we propose a hybrid mechanism utilizing oxide ion vacancies as well as hydroxyl groups. The surface processes during WGS over TiO_2 supported compounds can be written as:

$$CO + S_M \leftrightarrow CO_M \quad (12a)$$

$$H_2O + \text{"v"} \rightarrow H_2 + \text{"o"} \quad (12b)$$

$$H_2O + S_{Ti} \rightarrow H_2O_{Ti} \quad (12c)$$

$$H_2O_{Ti} + S_{Ti} \rightarrow OH_{Ti} + H_{Ti} \quad (12d)$$

$$OH_{Ti} + S_{Ti} \rightarrow O_{Ti} + H_{Ti} \quad (12e)$$

$$CO_M + \text{"o"} \rightarrow CO_2 + S_M + \text{"v"} \quad (12f)$$

$$CO_M + O_{Ti} \rightarrow CO_{2_{Ti}} + S_M \quad (12g)$$

$$CO_{2_{Ti}} \Leftrightarrow CO_2 + S_{Ti} \quad (12h)$$

$$H_{Ti} + H_{Ti} \rightarrow H_2 + 2S_{Ti} \quad (12i)$$

$$H_2 + S_M \Leftrightarrow H_{2_M} \quad (12j)$$

$$CO_2 + \text{"v"} \rightarrow CO + \text{"o"} \quad (12k)$$

$$CO_2 + S_{Ti} \rightarrow CO_{2_{Ti}} \quad (12l)$$

$$CO_{2_{Ti}} + S_{Ti} \rightarrow CO_{_{Ti}} + O_{Ti} \quad (12m)$$

$$CO_{_{Ti}} \rightarrow CO + S_{Ti} \quad (12n)$$

$$H_{2_M} + \text{"o"} \rightarrow H_2O + S_M \quad (12o)$$

$$H_{2_M} + O_{Ti} \rightarrow H_2O_{Ti} + S_M \quad (12p)$$

$$H_2O_{Ti} \Leftrightarrow H_2O + S_{Ti} \quad (12q)$$

The mechanism given by Eqs. 12a–12q can account for simultaneous utilization of oxide ion vacancies as well as the

surface hydroxyl groups. Several investigators including Lefferts and coworkers[21,22,55,56] have reported the possibility of utilization of oxide ion vacancies and the hydroxyl groups. The hydroxyl group formation and subsequent conversion to surface oxygen species was proposed. The mechanism proposed in this study makes a clear distinction between the surface sites and the related surface phenomena. The formation and utilization of oxide ion vacancies is given by the steps 12b, 12f, 12k, and 12o. Similarly, the consumption of the oxygen species formed over Ti in the support from the surface hydroxyl groups is given by Eqs. 12g and 12p.

In the aforementioned mechanism, there can be a possibility of interaction of adsorbed oxygen species on the oxide ion vacancy, ''o'', with the surface hydroxyl species, OH_{Ti}, by spill over. In such a case, the only possible step to carry the reaction further can be:

$$\text{“o”} + OH_{Ti} \rightarrow H_{Ti} + O_2 + \text{“v”} \tag{13}$$

Since no oxygen was observed during the experiments, the possibility of the above interactions was discarded. The evolved O_2 can react immediately with CO to give CO_2. But in that case, the H_2 evolution gets suppressed. Since this was not observed during the experiments, the possibility of the process given by Eq. 13 was discarded. Similarly, the interaction of H_2O directly with ''o'' can lead to the following sequences:

$$H_2O_{Ti} + \text{“o”} \rightarrow OH_{Ti} + \text{“O”H} \tag{14a}$$

$$OH_{Ti} + S_{Ti} \rightarrow O_{Ti} + H_{Ti} \tag{14b}$$

$$\text{“O”H} + S_{Ti} \rightarrow \text{“o”} + H_{Ti} \tag{14c}$$

The species produced by the above set of reactions are essentially those produced by the given mechanism. Therefore, Eqs. 12a–12q completely represent the surface phenomena occurring over TiO_2-based catalysts. Reducing the above set of equations to the working set by lumping of the several steps, we get the following:

$$CO + S_M \Leftrightarrow CO_M \tag{15a}$$

$$H_2O + \text{“v”} \rightarrow H_2 + \text{“o”} \tag{15b}$$

$$H_2O + S_{Ti} \rightarrow H_2 + o_{Ti} \tag{15c}$$

$$CO_M + \text{“o”} \rightarrow CO_2 + S_M + \text{“v”} \tag{15d}$$

$$CO_M + o_{Ti} \rightarrow CO_2 + S_M + S_{Ti} \tag{15e}$$

$$H_2 + S_M \Leftrightarrow H_{2_M} \tag{15f}$$

$$CO_2 + \text{“v”} \rightarrow CO + \text{“o”} \tag{15g}$$

$$CO_2 + S_{Ti} \rightarrow CO + o_{Ti} \tag{15h}$$

$$H_{2_M} + \text{“o”} \rightarrow H_2O + S_M + \text{“v”} \tag{15i}$$

$$H_{2_M} + o_{Ti} \rightarrow H_2O + S_M + S_{Ti} \tag{15j}$$

Solving for the above set of elementary reaction sequences, we get the rate expression as:

$$r = \frac{2(K_{15a}k_{15d}[CO] - K_{15f}k_{15i}[H_2])(k_{15b}[H_2O] + k_{15g}[CO_2])}{K_{15a}k_{15d}[CO] + K_{15f}k_{15i}[H_2] + (1 + K_{15a}[CO] + K_{15f}[H_2])(k_{15b}[H_2O] + k_{15g}[CO_2])} \tag{16}$$

The oxygen species in the catalyst formed as result of oxide ion vacancy and surface hydroxyl group are lumped together in the above analysis. Following the above modeling strategy, it may not be possible to determine the relative rates of consumption of hydroxyl groups and lattice oxygen utilization. The analysis can give the overall reaction kinetics but further spectroscopic studies might be required to determine the relative contribution of the different paths.

The details of the derivation and the underlying assumptions are discussed in detail in Appendix A.

Model validation and parameter estimation

The parameters appearing in the rate Eqs. 6, 10, and 16 were estimated using a non-linear regression algorithm based on Levenberg-Marquardt technique. Figure 1 shows the variation of CO concentration with temperature over different supported catalysts. The dotted line shows the equilibrium conversion at different temperatures. The symbols in the figure show the experimental data and the solid lines show the model predictions. Table 2 gives the various parameters obtained by regression. The parameters shown are those describing the forward WGS. In the temperature range of operation, where the reaction is far from equilibrium, the forward reaction dominates and the kinetic parameters for the forward reaction are sufficient to describe the variation of CO conversion with temperature. At higher temperatures, with an increase in the rate of reverse reaction, further kinetic analysis is required and the rate parameters have to be estimated on the basis of the complete rate equation over a larger range of temperatures.

The estimation of parameters for forward and backward reaction simultaneously increases the number of parameter and, hence, the reliability of the expression for describing the kinetics of the reaction decreases. Therefore, only the forward reaction parameters were estimated as a limiting case. A sensitivity analysis for the various parameters was carried out and parameters reported in Table 2 are the optimized values for the activation energies and the pre-exponential factors. The expressions for the equilibrium adsorption of CO and H_2 over the metal ions were taken directly from the literature to decrease the number of unknown parameters. The reversible adsorption used here are those over Pd or Pt metal. In the synthesized catalysts, Pd and Pt were substituted ionically. However, experimental evidences have been provided by Bera et al.[57] showing that the adsorption of CO over metal ions is same as that over the metals. Therefore, the following expressions for adsorption over metals were used.

Over Pd metal[58]: $K_{ads} = 10^{15.5} \exp(14{,}950/T)$

Over Pt metal[59]: $K_{ads} = 4.3 \times 10^4 \exp(16{,}165/T)$

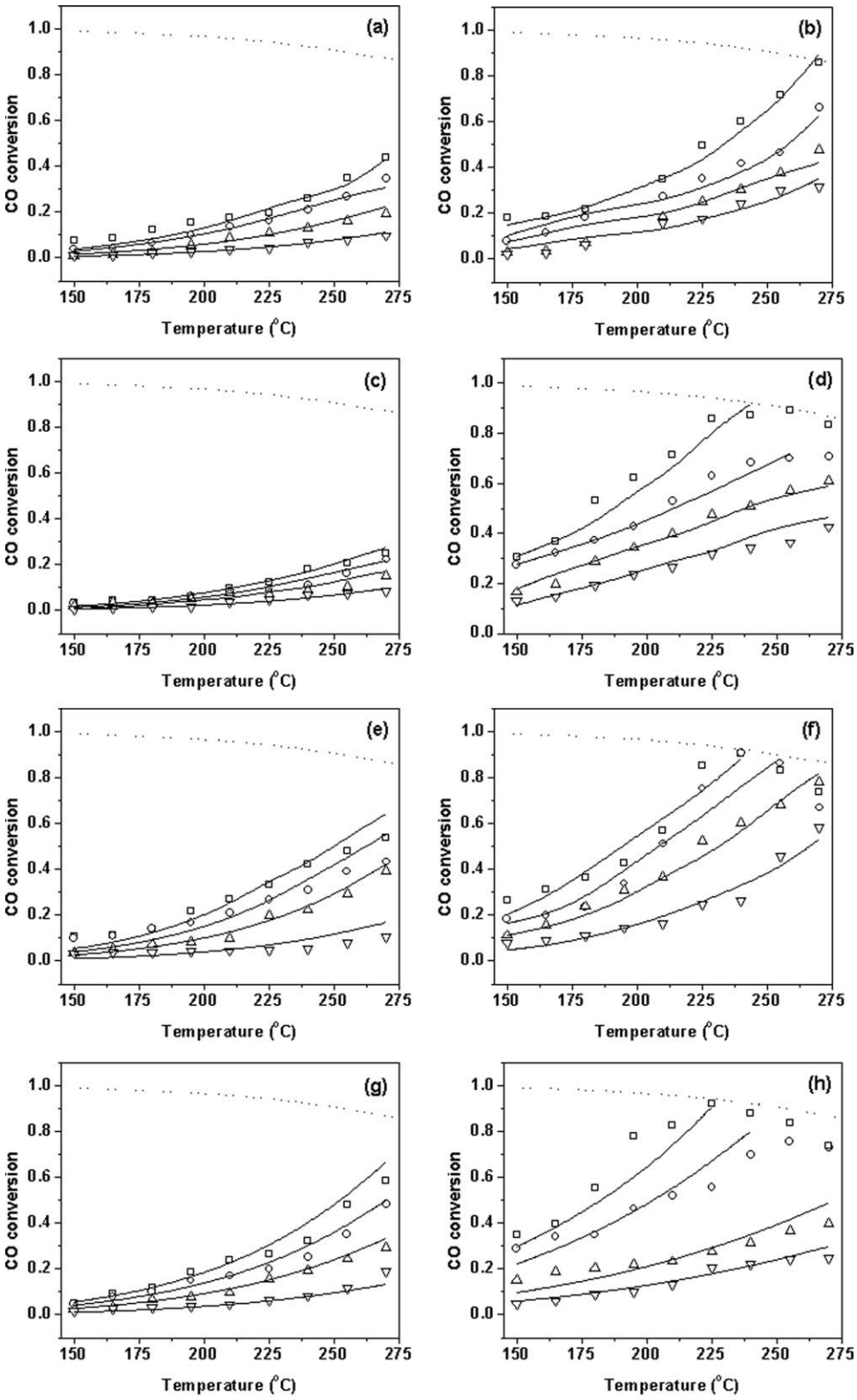

Figure 1. Variation of CO conversion with time over the different catalysts.

(a) $Ce_{0.83}Zr_{0.15}Pd_{0.02}O_{2-\delta}$, (b) $Ce_{0.83}Zr_{0.15}Pt_{0.02}O_{2-\delta}$, (c) $Ce_{0.83}Ti_{0.15}Pd_{0.02}O_{2-\delta}$, (d) $Ce_{0.83}Ti_{0.15}Pt_{0.02}O_{2-\delta}$, (e) $Zr_{0.98}Pd_{0.02}O_2$, (f) $Zr_{0.98}Pt_{0.02}O_2$, (g) $Ti_{0.98}Pd_{0.02}O_{2-\delta}$, (h) $Ti_{0.99}Pt_{0.01}O_{2-\delta}$.

Table 2. Optimized Rate Expressions for WGS Over Various Compounds

S. No	Compound	Parameter	Expression
1	$Ce_{0.83}Zr_{0.15}Pd_{0.02}O_{2-\delta}$	k_{1b}	$(1.25 \pm 0.04)\ \exp\{(-725 \pm 16)\}/T$
		k_{1c}	$(1.1 \pm 0.3)\ \exp\{(-4975 \pm 107)\}/T$
2	$Ce_{0.83}Zr_{0.15}Pt_{0.02}O_{2-\delta}$	k_{1b}	$(10.5 \pm 0.9)\ \exp\{(-2165 \pm 17)\}/T$
		k_{1c}	$(1.2 \pm 0.08)\ \exp\{(-3830 \pm 64)\}/T$
3	$Ce_{0.83}Ti_{0.15}Pd_{0.02}O_{2-\delta}$	k_{1b}	$(1.35 \pm 0.42)\ \exp\{(-1110 \pm 26)\}/T$
		k_{1c}	$(0.95 \pm 0.12)\ \exp\{(-5010 \pm 93)\}/T$
4	$Ce_{0.83}Ti_{0.15}Pt_{0.02}O_{2-\delta}$	k_{1b}	$(2.5 \pm 0.37)\ \exp\{(-1786 \pm 16)\}/T$
		k_{1c}	$(1.15 \pm 0.09)\ \exp\{(-3165 \pm 22)\}/T$
5	$Zr_{0.98}Pd_{0.02}O_2$	k_{9b}	$(0.1 \pm 0.01)\ \exp\{(-900 \pm 32)\}/T$
		k_{9c}	$(1.4 \pm 0.13)\ \exp\{(-5325 \pm 43)\}/T$
6	$Zr_{0.98}Pt_{0.02}O_2$	k_{9b}	$(0.15 \pm 0.02)\ \exp\{(-3800 \pm 29)\}/T$
		k_{9c}	$(0.07 \pm 0.01)\ \exp\{(-3054 \pm 16)\}/T$
7	$Ti_{0.98}Pd_{0.02}O_{2-\delta}$	k_{15b}	$(0.41 \pm 0.05)\ \exp\{(-1008 \pm 68)\}/T$
		k_{15d}	$(0.12 \pm 0.02)\ \exp\{(-3106 \pm 46)\}/T$
8	$Ti_{0.99}Pt_{0.01}O_{2-\delta}$	k_{15b}	$(1.15 \pm 0.8)\ \exp\{(-1109 \pm 23)\}/T$
		k_{15d}	$(0.19 \pm 0.03)\ \exp\{(-4750 \pm 21)\}/T$

From Figures 1a–h, it is clear that the activity of the Pt ion substituted material is superior to the Pd ion substituted material. Equilibrium conversions could be attained over all Pt ion substituted supports. The conversions with Pd-substituted supports did not exceed 40–50% for all the supports and required high weights of the catalyst. Equilibrium conversions were attained at a temperature of 240°C over Pt-substituted ZrO_2 and TiO_2. Different mechanisms including Langmuir-Hinshelwood and Eley-Rideal mechanism were tested for describing the variation of CO conversion with temperature. It was found that the mechanism proposed for a particular class of compounds only could describe the conversions. For other models, the optimization procedure resulted in negative activation energies and negative rate constants, similar to that observed in our previous study[29] indicating that these mechanisms did not occur over these catalysts.

We have previously tested different mechanisms for WGS over CeO_2-based Pd and Pt-substituted compounds. It was found that the classically described Langmuir-Hinshelwood and Eley-Rideal mechanisms are not able to describe the kinetics of the combustion synthesized compounds.[29] In this study, we have extended the idea to a series of compounds, belonging to different categories and have found that the proposed elementary processes indeed describe the reaction over the compounds.

The variation of CO conversion with the ratio of the weight of the catalysts and the molar flow rate is given in Figure 2. The slope of the plots in a small conversion range of 10–15% was used to estimate the rate of reaction assuming backmix conditions for small conversions. It can be seen that all the plots were linear at lower conversions. At higher conversions but lower temperatures, the plots remained linear. However, at higher temperatures and higher conversions, considerable deviation from linearity was observed. This was very prominent especially in case of Pt-substituted compounds.

Modeling the catalyst deactivation

The study of time variation of the catalyst activity becomes important to have an idea about the batch or regeneration time of the catalyst. Several phenomena have been proposed to describe the deactivation of the catalysts with time including poisoning, sintering, and fouling,[60] sintering being the most commonly observed in case of noble metal compounds.[61] In case of the ionic substitution of the metals in the support, the deactivation due to sintering is not possible. However, we have found support-dependent deactivation of the catalysts and the deactivation was found to be due to the formation of non-catalytic surface carbonate sites.[27] The formation of surface carbonates resulting in the loss of activity has been well reported.[62–68] In the reducible oxides, the formation of carbonates limits the rate at which ceria gets reoxidized.[65] This becomes especially relevant following Eqs. 1 through 6, where the reaction over the reducible CeO_2 compounds are influenced heavily by the reducibility of the support. Further, carbonates have high thermal stability and suppress the oxygen transfer,[62] and have been reported to be bound more strongly than oxygen.[69] The FTIR and XPS studies in our previous report[27] showed the presence of the carbonate group.

The carbonate formation and the subsequent deactivation was found to be the phenomena taking place entirely in the support. The direct interaction of CO with the support depends upon the acidic nature of the support. In any MO_2 system, when M is in +4 state, the M^{4+} ions are acidic in nature and the adsorbed CO or CO_2 can react with M^{4+} to give carbonate species. As a result, the catalytic activity of the compound decreases with time. Therefore, the decrease in the activity depends upon the acidic nature of the support.

For pure CeO_2 and La_2O_3, respective carbonates are formed. But, under the oxidizing conditions during WGS, the rate of formation of $Ce(CO_3)_2$ is negligible as compared to $LA_2(CO_3)_3$. La^{3+} is more basic as compared to Ce^{3+}. Therefore, substitution of La in CeO_2 results in the deterioration of the catalytic activity of the compound with time. Carbonates are not formed over Ti supports and, thus, Ti-substituted CeO_2 compounds show higher stability than that of unsubstituted or La-substituted compounds.[27]

To describe the deactivation of the catalyst, the concept of catalyst activity was used. Catalyst activity $a(t)$ is defined as the ratio of rate of reaction at any time t to the rate of reaction at time $t = 0$. Initially, $a(t) = 1$. The activity of the

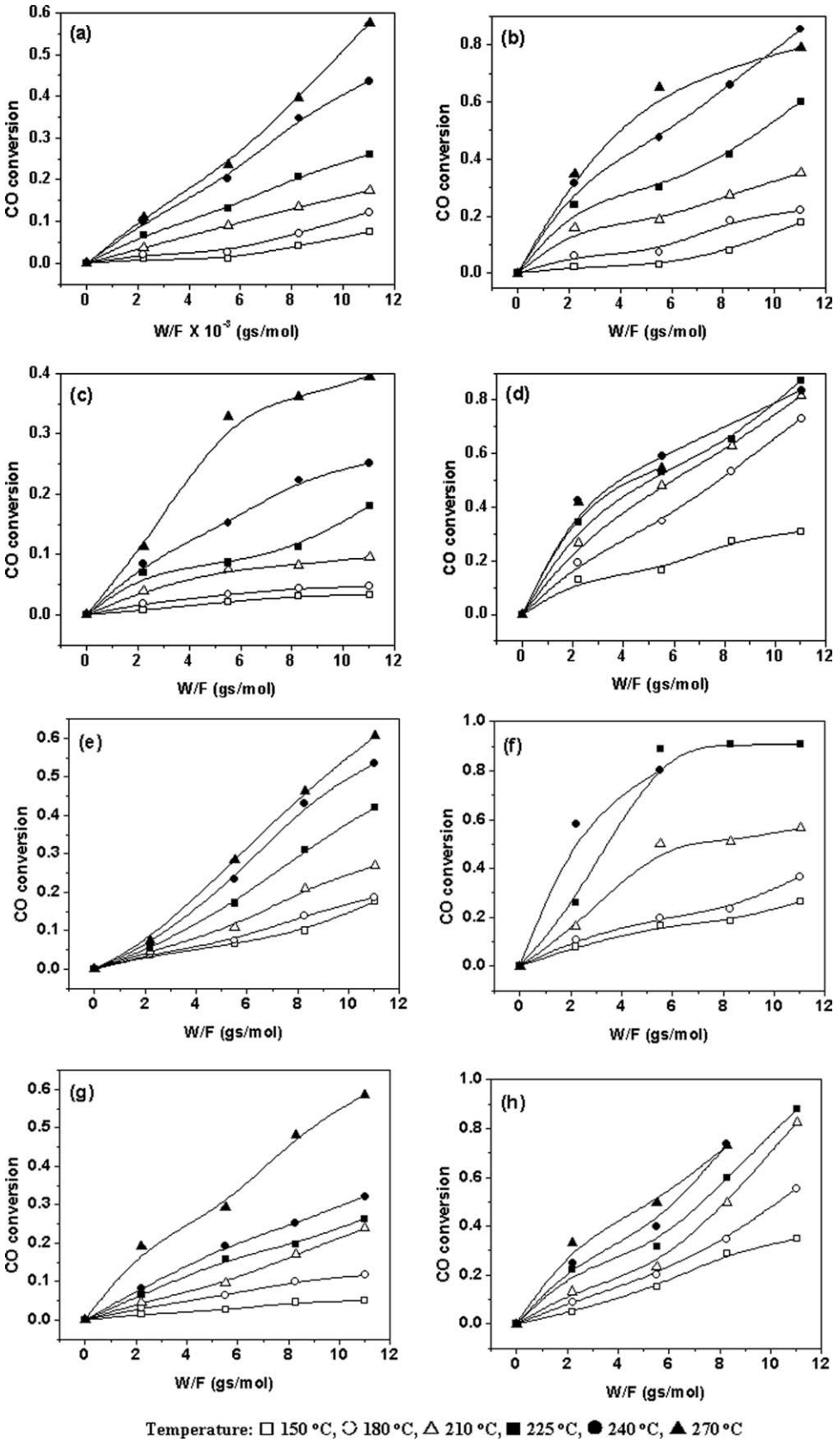

Figure 2. Variation of CO conversion with *W/F* ratio for the different catalyst.

(a) $Ce_{0.83}Zr_{0.15}Pd_{0.02}O_{2-\delta}$, (b) $Ce_{0.83}Zr_{0.15}Pt_{0.02}O_{2-\delta}$, (c) $Ce_{0.83}Ti_{0.15}Pd_{0.02}O_{2-\delta}$, (d) $Ce_{0.83}Ti_{0.15}Pt_{0.02}O_{2-\delta}$, (e) $Zr_{0.98}Pd_{0.02}O_2$, (f) $Zr_{0.98}Pt_{0.02}O_2$, (g) $Ti_{0.98}Pd_{0.02}O_{2-\delta}$, (h) $Ti_{0.99}Pt_{0.01}O_{2-\delta}$.

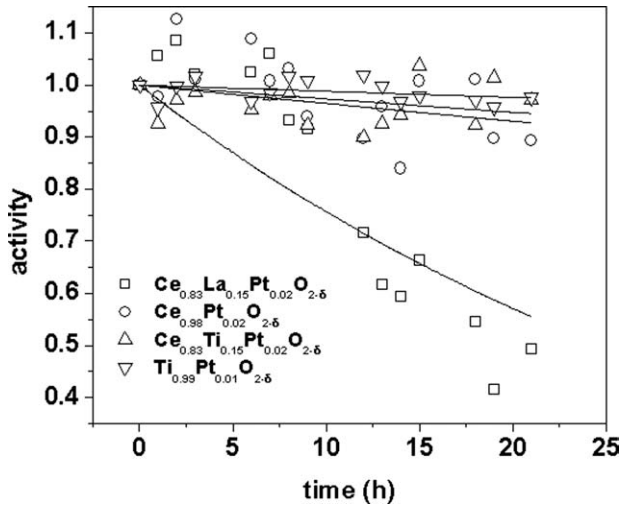

Figure 3. Variation of the catalyst activity with time.

catalyst decreases with time if the catalyst undergoes deactivation. Different expressions have been suggested for catalyst deactivation for different mechanisms. For deactivation by poisoning, a first order decay has been suggested to describe the deactivation kinetics.[60] Following equations show the variation of catalyst activity with time.

$$\frac{d}{dt}a(t) = -k_d a(t) \tag{17}$$

$$a(t) = a(0)\exp(-k_d t) = \exp(-k_d t) \tag{18}$$

where k_d is the deactivation constant. The magnitude of k_d gives an idea of the rate of deactivation of the catalyst. When the value of k_d is higher, the catalyst gets deactivated faster. The values of k_d were estimated by fitting the above equations to the experimental data. Figure 3 shows the variation of the catalyst activity with time. The solid lines show the model predictions. It can be seen that only La-substituted compound shows a large decrease in the activity. The decrease in the activity is nearly 45% within 20 h of operation. Other compounds show very less reduction in the activity. Table 3 gives the decay constant k_d for the various catalysts. The value of k_d for La-substituted compound is one order of magnitude higher than that of the others. Although a large scatter can be observed in the data given in Figure 3, the model has correctly captured the deactivation trends. From the XPS studies, it was found that the carbonate formation followed the order $Ce_{0.83}La_{0.15}Pt_{0.02}O_{2-\delta} > Ce_{0.98}Pt_{0.02}O_{2-\delta} > Ce_{0.83}Ti_{0.15}Pt_{0.02}O_{2-\delta} > Ti_{0.99}Pt_{0.01}O_{2-\delta}$. The same trend has been obtained from the deactivation kinetic model.

Table 3. First Order Decay Constants for the Catalyst Deactivation

S. No	Compound	K_d ($\times 10^3$)
1	$Ce_{0.83}La_{0.15}Pt_{0.02}O_{2-\delta}$	28 ± 4
2	$Ce_{0.98}Pt_{0.02}O_{2-\delta}$	3.6 ± 0.4
3	$Ce_{0.83}Ti_{0.15}Pt_{0.02}O_{2-\delta}$	2.7 ± 0.1
4	$Ti_{0.99}Pt_{0.01}O_{2-\delta}$	1.2 ± 0.04

Conclusions

Pd and Pt ion substituted compounds were found to be active for catalyzing WGS. WGS over CeO_2-based solid solutions was described using the dual site mechanism. Redox Ce^{3+}-Ce^{4+} transitions with changes in Pt oxidation states were observed. WGS over ZrO_2-based compounds was described using surface hydroxyl mechanism. Pt was found to get reduced to metallic state and hydroxyl groups were proposed to play a key role for the high activity of the compound. A hybrid mechanism incorporating both dual site mechanism and surface hydroxyl mechanism was found to describe WGS activity of TiO_2 supported compounds. The activity of Pt-substituted compounds was higher than that of Pd-substituted compounds and equilibrium conversions were achieved by Pt substitution.

Acknowledgments

The authors are grateful to the Department of Science and Technology, Government of India, for funding. G.M. gratefully acknowledges the Government of India, for the Swarnajayanti fellowship. P.A.D. gratefully acknowledges Bristol-Myers Squibb for the fellowship.

Literature Cited

1. Campbell CT, Daube KA. A surface science investigation of the water-gas shift reaction on Cu(111). *J Catal*. 1987;104:109–119.
2. Chinchen GC, Spencer MS. Sensitive and insensitive reactions on copper catalysts: the water-gas shift reaction and methanol synthesis from carbon dioxide. *Catal Today*. 1991;10:293–301.
3. Sekizawa K, Sei-ichi Y, Eguchi K, Arai H. Selective removal of CO in methanol reformed gas over Cu-supported mixed metal oxides. *Appl Catal A: Gen*. 1998;169:291–297.
4. Utaka T, Sekizawa K, Eguchi K. CO removal by oxygen-assisted water gas shift reaction over supported Cu catalysts. *Appl Catal A: Gen*. 2000;194-195:21–26.
5. Tanaka Y, Utaka T, Kikuchi R, Sasaki K, Eguchi K. Water-gas shift reaction over Cu-based mixed oxides for CO removal from reformed fuels. *Appl Catal A: Gen*. 2003;242:287–295.
6. Gines MJL, Amadeo N, Laborde M, Apestegufa CR. Activity and structure-sensitivity of the water-gas shift reaction over Cu-Zn-Al mixed oxide catalysts. *Appl Catal A: Gen*. 1995;131:283–296.
7. Corti CW, Holliday RJ, Thompson DT. Commercial aspects of gold catalysis. *Appl Catal A: Gen*. 2005;291:253–261.
8. Ratnasamy C, Wagner JP. Water-gas shift catalysis. *Catal Rev*. 2009; 51:325–440.
9. Dictor R. A kinetic study of the water-gas shift reaction over Rh/Al_2O_3. *J Catal*. 1987;106:458–463.
10. Shelef M, Gandhi HS. Ammonia formation in the catalytic reduction of nitric oxide. III. The role of water gas shift, reduction by hydrocarbons, and steam reforming. *Ind Eng Chem Prod Res Dev*. 1974; 13:80–85.
11. Olympiou GG, Kalamaras CM, Zeinalipour-Yazdi CD, Efstathiou AM. Mechanistic aspects of the water-gas shift reaction on alumina-supported noble metal catalysts: In situ DRIFTS and SSITKA-mass spectrometry studies. *Catal Today*. 2007;127:304–318.
12. Radhakrishnan R, Willigan RR, Dardas Z, Vanderspurt TH. Water gas shift activity of noble metals supported on ceria-zirconia oxides. *AIChE J*. 2006;52:1888–1894.
13. Radhakrishnan R, Willigan RR, Dardas Z, Vanderspurt TH. Water gas shift activity and kinetics of Pt/Re catalysts supported on ceria-zirconia oxides. *Appl Catal B: Environ*. 2006;66:23–28.
14. Fonseca AA, Fisher JM, Ozkaya D, Shannon MD, Thompsett D. Ceria-Zirconia supported Au as highly active low temperature water-gas shift catalyst. *Topic Catal*. 2007;44:223–235.
15. Fu Q, Saltsberg H, Flytzani-Stephanopoulos M. Active non-metallic Au and Pt species on ceria-based water-gas shift catalyst. *Science*. 2003;301:935–938.

16. Rodrigues JA, Ma S, Liu P, Hrbek J, Evens J, Perez M. Activity of CeO_2 and TiO_2 nanoparticles grown on Au(111) in the water-gas shift reaction. *Science*. 2007;318:1757–1760.
17. Germani G, Schuurman Y. Water-gas shift kinetics over μ-structured $Pt/CeO_2/Al_2O_3$ catalysts. *AIChE J*. 2006;52:1806–1813.
18. Panagiotopoulou P, Papavasiliou J, Avogouropolous G, Ioannides T, Kondarides DI. Water-gas shift activity of doped Pt/CeO_2 catalysts. *Chem Eng J*. 2007;134:16–22.
19. Panagiotopoulou P, Christodoulakis A, Kondarides DI, Boghosian S. Particle size effects on the reducibility of titanium dioxide and its relation to the water-gas shift activity of Pt/TiO_2 catalysts. *J Catal*. 2006;240:114–125.
20. Boaro M, Vicario M, Llorca J, de Leitenburg C, Dolcetti G, Trovarelli A. A comparative study of water-gas shift reaction over gold and platinum on supported ZrO_2 and CeO_2-ZrO_2. *Appl Catal B: Environ*. 2009;88:272–282.
21. Azzam KG, Babich IV, Seshan K, Lefferts L. Bifunctional catalysts for single-stage water-gas shift reaction in fuel cell applications. Part 1. Effect of the support on the reaction sequence. *J Catal*. 2007; 251:153–162.
22. Azzam KG, Babich IV, Seshan K, Lefferts L. A bifunctional catalyst for the single-stage water-gas shift reaction in fuel cell applications. Part 2. Roles of the support and promoter on catalyst activity and stability. *J Catal*. 2007;251:163–171.
23. Deshpande PA, Hegde MS, Madras G. Pd and Pt ions as highly active sites for the water-gas shift reaction over combustion synthesized zirconia and zirconia-modified ceria. *Appl Catal B: Environ*. In press.
24. Bakhmutsky K, Zhou G, Timothy S, Gorte RJ. The water-gas shift reaction on Pd/ceria-praseodymia: the effect of redox thermodynamics. *Catal Lett*. 2009;129:61–65.
25. Deng W, Flytzani-Stephanopoulos M. On the issue of the deactivation of Au-ceria and Pt-ceria water-gas shift catalysts in practical fuel-fell applications. *Angew Chem Int Ed*. 2006;45:2285–2289.
26. Kim CH, Thompson LT. Deactivation of Au/CeOx water gas shift catalysts. *J Catal*. 2005;230:66–74.
27. Sharma S, Deshpande PA, Hegde MS, Madras G. Nondeactivating nanosized ionic catalysts for water-gas shift reaction. *Ind Eng Chem Res*. 2009;48:6535–6543.
28. Hegde MS, Madras G, Patil KC. Nobel metal ionic catalysts. *Acc Chem Res*. 2009;42:704–712.
29. Deshpande PA, Hegde MS, Madras G. A mechanistic model for the water gas shift reaction over noble metal substituted ceria. *AIChE J*. In press. DOI: 10.1002/aic.12062.
30. Baidya T, Marimuthu A, Hegde MS, Ravishankar N, Madras G. Higher catalytic activity of nano-$Ce_{1-x-y}Ti_xPd_yO_2$ compared to nano-$Ce_{1-x}Pd_xO_2$ for CO oxidation and N_2O and NO reduction by CO: role of oxide ion vacancy. *J Phys Chem C*. 2007;111:830–839.
31. Baidya T, Dutta G, Hegde MS, Waghmare UV. Noble metal ionic catalysts: correlation of increase in CO oxidation activity with increasing effective charge on Pd ion in Pd ion substituted $Ce_{1-x}M_xO_{2-\delta}$ (M = Ti, Zr and Hf). *Dalton Trans*. 2009;3:455–464.
32. Dutta G, Waghmare UV, Baidya T, Hegde MS. Hydrogen spillover on CeO_2/Pt: enhanced storage of active hydrogen. *Chem Mater*. 2007;19:6430–6436.
33. Sharma S, Hegde MS. Pt metal-CeO_2 interaction: direct observation of redox coupling between $Pt^0/Pt^{2+}/Pt^{4+}$ and Ce^{4+}/Ce^{3+} states in $Ce_{0.98}Pt_{0.02}O_{2-\delta}$ catalyst by a combined electrochemical and x-ray photoelectron spectroscopy study. *J Chem Phys*. 2009;130: 114706.
34. Pierre D, Deng W, Flytzani-Stephanopoulos M. The importance of strongly bound Pt-CeO_x species for the water-gas shift reaction: catalyst activity and stability evaluation. *Topic Catal*. 2007;3-4:363–373.
35. Becker E, Thormahlen P, Maunula T, Saupanki A, Skolungth M. Low temperature activity of CO oxidation over diesel oxidation catalysts studied by high throughput screening and DRIFT spectroscopy. *Topic Catal*. 2007;42-43:421–424.
36. Jacobs G, Davis BH. Low temperature water-gas shift: applications of modified SSITKA-DRIFTS method under conditions of H_2 cofeeding over metal/ceria and related oxides. *Appl Catal A: Gen*. 2007;33:192–201.
37. Tibiletti D, Meuneir FC, Goguet A, Reid D, Burch R, Boaro M, Vicario M, Trovarelli A. An investigation of possible mechanisms for the water-gas shift reaction over ZrO_2-supported Pt catalysts. *J Catal*. 2006;244:183–191.
38. Fisher IA, Bell AT. A mechanistic study of methanol decomposition over Cu/SiO_2, ZrO_2/SiO_2 and $Cu/ZrO_2/SiO_2$. *J Catal*. 1999;184:357–376.
39. Zhu J, Albertsma S, Van Ommen JG, Lefferts L. Role of surface defects in activation of O_2 and N_2O on ZrO_2 and yttrium-stabilized ZrO_2. *J Phys Chem B*. 2005;109:9550–9555.
40. Graf PO, de Vlieger DJM, Mojet BL, Lefferts L. New insights in reactivity of hydroxyl groups in water gas shift reaction on Pt/ZrO_2. *J Catal*. 2009;262:181–187.
41. Wokaun A, Weigel J, Kilo M, Baiker A. Metal/Zirconia catalysts for synthesis of methanol: characterization by vibrational spectroscopy. *Fresenius J Anal Chem*. 1994;349:71–75.
42. Schild C, Wokaun A, Baiker A. On the mechanism of CO and CO_2 hydrogenation reactions on zirconia-supported catalysts: a diffused reflectance FTIR study. Part II. Surface species on copper/zirconia catalysts: implications for methanol synthesis selectivity. *J Mol Catal*. 1990;60:243–254.
43. Koeppel RA, Baiker A, Schild C, Wokaun A. Carbon dioxide hydrogenation over Au/ZrO_2 catalysts from amorphous precursors: catalytic reaction mechanism. *J Chem Soc Faraday Trans*. 1991;87: 2821–2128.
44. Kilo M, Weigel J, Wokaun A, Koeppel RA, Stoeckli A, Baiker A. Effect of the addition of chromium- and manganese oxides on structural and catalytic properties of copper/zirconia catalysts for the synthesis of methanol from carbon dioxide. *J Mol Catal A: Chem*. 1997;2-3: 169–184.
45. Tang Q, Hong Q, Liu Z. CO_2 fixation into methanol at Cu/ZrO_2 interface from first principles kinetic Monte Carlo. *J Catal*. 2009;263:114–122.
46. Duttta G, Waghmare UV, Baidya T, Hegde MS, Priolkar KR, Sarode PR. Origin of enhanced reducibility/oxygen storage capacity of $Ce_{1-x}Ti_xO_2$ compared to CeO_2 or TiO_2. *Chem Mater*. 2006;18: 3249–3256.
47. Kalamaras CM, Panagiotopoulou P, Kondarides DI, Efstathiou AM. Kinetic and mechanistic studies of the water-gas shift reaction on Pt/TiO_2 catalyst. *J Catal*. 2009;264:117–129.
48. Panagiotopoulou P, Kondarides DI. Effects of alkali promotion of TiO_2 on the chemisorptive properties and water-gas shift activity of supported noble metal catalysts. *J Catal*. 2009;267:57–66.
49. Panagiotopoulou P, Kondarides DI. Effect of morphological characteristics of TiO_2 supported noble metal catalysts on their activity for the water-gas shift reaction. *J Catal*. 2004;225:327–336.
50. Schaub R, Thostrup P, Lopez N, Lagsgaard E, Stensgaard I, Norskov JK, Besenbacher F. Oxygen vacancies as active sites for water dissociation on rutile TiO_2 (110). *Phys Rev Lett*. 2001;87:266104.
51. Brookes IM, Muryn CA, Thornton G. Imaging water dissociation on TiO_2 (110). *Phys Rev Lett*. 2001;87:266103.
52. Boccuzzi F, Chiorino A, Manzoli M, Andreeva D, Tabakova T. FTIR study of low-temperature water-gas shift reaction on Au/Fe_2O_3 and Au/TiO_2 catalysts. *J Catal*. 1999;188:176–185.
53. Gonzales ID, Navarro RM, Galvan MCA, Rosa F, Fierro JLG. Performance enhancement in the water-gas shift reaction of Pt deposited over a cerium modified TiO_2 support. *Catal Commun*. 2008;9: 1759–1765.
54. Nagaveni K, Hegde MS, Ravishankar N, Subbanna GN, Madras G. Synthesis and structure of nanocrystalline TiO_2 with lower band gap showing higher photocatalytic activity. *Langmuir*. 2004;20:2900–2907.
55. Azzam KG, Babich IV, Seshan K, Lefferts L. Single stage water gas shift conversion over Pt/TiO_2: problem of catalyst deactivation. *Appl Catal A: Gen*. 2008;338:66–71.
56. Liu P, Rodriguez JA. Water-gas shift reaction on metal nanoparticles and surfaces. *J Chem Phys*. 2007;126:164705.
57. Bera P, Patil KC, Jayaram V, Subbanna GN, Hegde MS. Ionic dispersion of Pt and Pd ions by combustion method: effect of metal-ceria interaction on catalytic activities for NO reduction and CO and hydrocarbon oxidation. *J Catal*. 2000;196:293–301.
58. Henry CR, Chapon C, Duriz C. Adsorption-desorption kinetics on epitaxially oriented palladium clusters. *Z Phys D: Atoms Mol Clusters*. 1991;19:347–351.
59. Sexton BA, Hughes AE. A comparison of weak molecular adsorption of organic molecules on clean copper and platinum surfaces. *Surf Sci*. 1984;140:227–248.
60. Fogler HS. *Elements of Chemical Reaction Engineering*, 3rd ed. New Delhi: Prentice Hall of India, 2005.

61. Kucaynski GC. *Material Science Research*, Vol. 10. New York: Plenum Press, 1975.
62. Djinovic P, Batista J, Pintar A. WGS reaction over nanostructured CuO-CeO_2 catalysts prepared by hard template method: characterization, activity and deactivation. *Catal Today*. 2009; doi: 10.1016/j.cattod. 2009.07.009.
63. El-Moemen AA, Karpenko A, Denkwitz Y, Behm RJ. Activity, stability and deactivation behavior of Au/CeO_2 catalysts in the water gas shift reaction at increased reaction temperature (300°C). *J Power Sourc*. 2009;190:64–75.
64. Liu X, Ruettinger W, Xu X, Farrauto R. Deactivation of Pt/CeO_2 water-gas shift catalysts due to shutdown/startup modes for fuel cell applications. *Appl Catal B: Environ*. 2005;56:69–75.
65. Hilaire S, Wang X, Luo T, Gorte RJ, Wagner J. A comparative study of water-gas shift reaction over ceria-supported metallic catalysts. *Appl Catal A: Gen*. 2004;258:271–276.
66. Gorte RJ, Zhao S. Studies of the water-gas-shift reaction with ceria-supported precious metals. *Catal Today*. 2005;104:18–24.
67. Zhao S, Luo T, Gorte RJ. Deactivation of the water-gas-shift activity of Pd/ceria by Mo. *J Catal*. 2004;221:413–420.
68. Wang X, Gorte RJ, Wagner JP. Deactivation mechanisms for Pd/ceria during the water-gas shift reaction. *J Catal*. 2002;212:225–230.
69. Marban G, Lopez I, Valdes-Solis T. Preferential oxidation of CO by CuO_x/CeO_2 nanocatalysts prepared by SACOP. Mechanisms of deactivation under the reactant stream. *Appl Catal A: Gen*. 2009; 361:160–169.

Appendix A: Derivation of the Various Rate Expressions for the WGS Over the Different Supports

A: Rate expression for dual site mechanism (CeO_2-based catalysts)

Equations 1a and 1d represent the reversible adsorption of CO and H_2 over the metal ion, respectively. If k_{1a} and k_{-1a} represent the forward and reverse rate constants for step 1a, respectively, and the equilibrium adsorption constant K_{1a} is defined as:

$$K_{1a} = k_{1a}/k_{-1a} \tag{A1}$$

then at equilibrium,

$$r_{1a} = k_{1a}[CO]\theta_v - k_{-1a}\theta_{CO_M} = 0 \tag{A2}$$

where θ_v represents the fraction of the metal sites unoccupied, θ_{CO_M}, the fraction of the metal sites occupied by CO and [CO], the concentration of CO.

Similarly,

$$r_{1d} = k_{1d}[H_2]\theta_v - k_{-1d}\theta_{H_{2_M}} = 0 \tag{A3}$$

From Eqs. A2 and A3

$$\theta_{CO_M} = K_{1a}[CO]\theta_v \tag{A4}$$

$$\theta_{H_{2_M}} = K_{1d}[H_2]\theta_v \tag{A5}$$

The site balance over the metal,

$$\theta_v + \theta_{CO_M} + \theta_{H_{2_M}} = 1 \tag{A6}$$

Solving Eqs. A4, A5, and A6 simultaneously,

$$\theta_{CO_M} = \frac{K_{1a}[CO]}{1 + K_{1a}[CO] + K_{1d}[H_2]} \tag{A5a}$$

$$\theta_{H_{2_M}} = \frac{K_{1d}[H_2]}{1 + K_{1a}[CO] + K_{1d}[H_2]} \tag{A6a}$$

The effective surface reaction rate is

$$r = k_{1c}\theta_{CO_M}\theta_{oov} - k_{1f}\theta_{H_{2_M}}\theta_{oov} \tag{A7}$$

$$r = (k_{1a}\theta_{CO_M} - k_{1f}\theta_{H_{2_M}})\theta_{oov} \tag{A8}$$

where θ_{oov} gives the fraction of sites on support occupied by the oxide ion vacancies. If θ_{vov} represents the fraction of sites on support unoccupied then the site balance on support,

$$\theta_{oov} + \theta_{vov} = 1 \tag{A9}$$

Applying quasi-steady state approximation,

$$k_{1b}[H_2O]\theta_{vov} + k_{1e}[CO_2]\theta_{vov} = k_{1c}\theta_{CO_M}\theta_{oov} + k_{1f}\theta_{H_{2_M}}\theta_{oov} \tag{A10}$$

Solving for θ_{oov} using Eqs. A9 and A10,

$$\theta_{oov} = \frac{(1 + K_{1a}[CO])(1 + K_{1d}[H_2])(k_{1b}[H_2O] + k_{1e}[CO_2])}{(1 + K_{1a}[CO])(1 + K_{1d}[H_2])(k_{1b}[H_2O] + k_{1e}[CO_2]) + (1 + K_{1d}[H_2])K_{1a}k_{1c}[CO] + (1 + K_{1a}[CO])K_{1d}k_{1f}[H_2]} \tag{A10a}$$

Substituting the values of θ_{CO_M}, $\theta_{H_{2M}}$, and θ_{oov} from Eqs. A5a, A6a, and A10a the rate expression is

$$r = \frac{\{K_{1a}k_{1c}[CO](1 + K_{1d}[H_2]) - K_{1d}k_{1f}[H_2](1 + K_{1a}[CO])\}(k_{1b}[H_2O] + k_{1e}[CO_2])}{(1 + K_{1a}[CO])(1 + K_{1d}[H_2])(k_{1b}[H_2O] + k_{1e}[CO_2]) + (1 + K_{1d}[H_2])K_{1a}k_{1c}[CO] + (1 + K_{1a}[CO])K_{1d}k_{1f}[H_2]} \tag{A11}$$

Equation A11 gives the required rate expression. The limiting rate expression for forward water gas shift reaction is given as:

$$r = \frac{K_{1a}k_{1b}k_{1c}[CO][H_2O]}{K_{1a}k_{1c}[CO] + k_{1b}[H_2O](1 + K_{1a}[CO])}. \tag{A12}$$

B: Rate expression for surface hydroxyl mechanism (ZrO_2-based catalysts)

The equilibrium adsorption of CO and H_2 over the metal is given by:

$$\theta_{CO_M} = \frac{K_{9a}[CO]}{1 + K_{9a}[CO] + K_{9d}[H_2]} \quad \text{(A13)}$$

$$\theta_{H_{2_M}} = \frac{K_{9d}[H_2]}{1 + K_{9a}[CO] + K_{9d}[H_2]} \quad \text{(A14)}$$

Site balance over Zr,

$$\theta_{Zr_v} + \theta_{ZrO} = 1 \quad \text{(A15)}$$

where θ_{Zr_v} is the fraction of Zr sites that are vacant and θ_{ZrO} is the fraction of Zr sites occupied by the intermediate species formed due to surface hydroxyl decomposition.

Pseudo steady state approximation on θ_{ZrO} gives,

$$k_{9b}[H_2O]\theta_{Zr_v} + k_{9c}\theta_{CO_M}\theta_{ZrO} + k_{9e}[CO_2]\theta_{Zr_v} - k_{9f}\theta_{H_{2_M}}\theta_{ZrO} = 0 \quad \text{(A16)}$$

Solving Eqs. A15 and A16,

$$\theta_{ZrO} = \left(\frac{k_{9b}[H_2O] + k_{9e}[CO_2]}{k_{9c}\theta_{CO_M} + k_{9f}\theta_{H_{2_M}}}\right)\theta_{Zr_v} \quad \text{(A17)}$$

$$\theta_{Zr_v} = \frac{k_{9c}\theta_{CO_M} + k_{9f}\theta_{H_{2_M}}}{k_{9c}\theta_{CO_M} + k_{9f}\theta_{H_{2_M}} + k_{9b}[H_2O] + k_{9e}[CO_2]} \quad \text{(A18)}$$

The rate of reaction is given by,

$$r = k_{9c}\theta_{CO_M}\theta_{ZrO} + k_{9f}\theta_{H_{2_M}}\theta_{ZrO} \quad \text{(A19)}$$

Substituting the expression for θ_{ZrO} in Eq. A19,

$$r = \frac{\left(k_{9c}\theta_{CO_M} - k_{9f}\theta_{H_{2_M}}\right)(k_{9b}[H_2O] + k_{9e}[CO_2])}{k_{9c}\theta_{CO_M} + k_{9f}\theta_{H_{2_M}} + k_{9b}[H_2O] + k_{9e}[CO_2]} \quad \text{(A20)}$$

Using the expressions for the adsorption equilibrium from Eqs. A13 and A14,

$$r = \frac{(k_{9c}K_{9a}[CO] - k_{9f}K_{9d}[H_2])(k_{9b}[H_2O] + k_{9e}[CO_2])}{k_{9c}K_{9a}[CO] - k_{9f}K_{9d}[H_2] + (1 + K_{9a}[CO] + K_{9d}[H_2])(k_{9b}[H_2O] + k_{9e}[CO_2])} \quad \text{(A21)}$$

Equation A21 gives the required rate expression. The limiting rate expression for the forward water gas shift reaction is given as:

$$r = \frac{K_{9a}k_{9b}k_{9c}[CO][H_2O]}{K_{9a}k_{9c}[CO] + k_{9b}[H_2O](1 + K_{9a}[CO])} \quad \text{(A22)}$$

C: Rate expression for hybrid mechanism (TiO_2-based catalysts)

The expressions for reversible adsorption of CO and H_2 over the noble metal ion is given as:

$$\theta_{CO} = \frac{K_{15a}[CO]}{1 + K_{15a}[CO] + K_{15f}[H_2]} \quad \text{(A23)}$$

$$\theta_{H_2} = \frac{K_{15f}[H_2]}{1 + K_{15a}[CO] + K_{15f}[H_2]} \quad \text{(A24)}$$

The rate of reaction is given as:

$$r = r_{15d} + r_{15e} - r_{15i} - r_{15j} \quad \text{(A25)}$$

$$r = k_{15d}\theta_{CO_M}\theta_{oov} + k_{15e}\theta_{CO_M}\theta_{oTi} - k_{15i}\theta_{H_{2_M}}\theta_{oov} - k_{15j}\theta_{H_{2_M}}\theta_{oTi} \quad \text{(A26)}$$

The balance over oxygen species over the support "o" is given as:

$$k_{15b}[H_2O]\theta_{vov} - k_{15d}\theta_{CO_M}\theta_{oov} + k_{15g}[CO_2] - k_{15i}\theta_{H_{2_M}}\theta_{oov} = 0 \quad \text{(A27)}$$

$$\theta_{oov} = \left(\frac{k_{15b}[H_2O] + k_{15g}[CO_2]}{k_{15d}\theta_{CO_M} + k_{15i}\theta_{H_{2_M}}}\right)\theta_{vov} \quad \text{(A28)}$$

Similarly, the balance over o_{Ti} gives

$$\theta_{oTi} = \left(\frac{k_{15c}[H_2O] + k_{15h}[CO_2]}{k_{15e}\theta_{CO_M} + k_{15j}\theta_{H_{2_M}}}\right)\theta_{vTi} \quad \text{(A29)}$$

The balance on oxide ion vacancies gives

$$\theta_{vov} + \theta_{oov} = 1 \quad \text{(A30)}$$

Using Eqs. A28 and A30 we get the expression for θ_{vov}

$$\theta_{vov} = \frac{k_{15d}\theta_{CO_M} + k_{15i}\theta_{H_{2_M}}}{k_{15d}\theta_{CO_M} + k_{15i}\theta_{H_{2_M}} + k_{15b}[H_2O] + k_{15g}[CO_2]} \quad \text{(A31)}$$

Similarly,

$$\theta_{vTi} = \frac{k_{15e}\theta_{CO_M} + k_{15j}\theta_{H_{2_M}}}{k_{15e}\theta_{CO_M} + k_{15j}\theta_{H_{2_M}} + k_{15c}[H_2O] + k_{15h}[CO_2]} \quad \text{(A31a)}$$

From the above expressions and the adsorption equilibrium relations (Eqs. A23 and A24), we obtain the following expression:

$$r_4 = \frac{k_{15d}\theta_{CO_M}(k_{15b}[H_2O] + k_{15g}[CO_2])}{k_{15d}\theta_{CO_M} + k_{15i}\theta_{H_{2_M}} + k_{15b}[H_2O] + k_{15g}[CO_2]} \quad \text{(A32)}$$

$$r_5 = \frac{k_{15e}\theta_{CO_M}(k_{15c}[H_2O] + k_{15h}[CO_2])}{k_{15e}\theta_{CO_M} + k_{15j}\theta_{H_{2_M}} + k_{15c}[H_2O] + k_{15h}[CO_2]} \quad \text{(A33)}$$

$$r_9 = \frac{k_{15i}\theta_{H_{2_M}}(k_{15b}[H_2O] + k_{15g}[CO_2])}{k_{15d}\theta_{CO_M} + k_{15i}\theta_{H_{2_M}} + k_{15b}[H_2O] + k_{15g}[CO_2]} \quad \text{(A34)}$$

$$r_{10} = \frac{k_{15j}\theta_{H_{2_M}}(k_{15c}[H_2O] + k_{15h}[CO_2])}{k_{15e}\theta_{CO_M} + k_{15j}\theta_{H_{2_M}} + k_{15c}[H_2O] + k_{15h}[CO_2]} \quad \text{(A35)}$$

Substituting Eqs. A32–A35 in Eq. A30 we get

$$r = \frac{k_{15d}\theta_{CO_M}(k_{15b}[H_2O] + k_{15g}[CO_2])}{k_{15d}\theta_{CO_M} + k_{15i}\theta_{H_{2_M}} + k_{15b}[H_2O] + k_{15g}[CO_2]} + \frac{k_{15e}\theta_{CO_M}(k_{15c}[H_2O] + k_{15h}[CO_2])}{k_{15e}\theta_{CO_M} + k_{15j}\theta_{H_{2_M}} + k_{15c}[H_2O] + k_{15h}[CO_2]} - \frac{k_{15i}\theta_{H_{2_M}}(k_{15b}[H_2O] + k_{15g}[CO_2])}{k_{15d}\theta_{CO_M} + k_{15i}\theta_{H_{2_M}} + k_{15b}[H_2O] + k_{15g}[CO_2]} - \frac{k_{15j}\theta_{H_{2_M}}(k_{15c}[H_2O] + k_{15h}[CO_2])}{k_{15e}\theta_{CO_M} + k_{15j}\theta_{H_{2_M}} + k_{15c}[H_2O] + k_{15h}[CO_2]} \quad \text{(A36)}$$

Setting $k_{15b} = k_{15c}$, $k_{15d} = k_{15e}$, $k_{15g} = k_{15h}$, and $k_{15i} = k_{15j}$

$$r = \frac{2(k_{15d}\theta_{CO_M} - k_{15i}\theta_{H_{2_M}})(k_{15b}[H_2O] + k_{15g}[CO_2])}{k_{15d}\theta_{CO_M} + k_{15i}\theta_{H_{2_M}} + k_{15b}[H_2O] + k_{15g}[CO_2]} \quad \text{(A37)}$$

Substituting Eqs. A23 and A24 in Eq. A37, we get the required rate expression as:

$$r = \frac{2(K_{15a}k_{15d}[CO] - K_{15f}k_{15i}[H_2])(k_{15b}[H_2O] + k_{15g}[CO_2])}{K_{15a}k_{15d}[CO] + K_{15f}k_{15i}[H_2] + (1 + K_{15a}[CO] + K_{15f}[H_2])(k_{15b}[H_2O] + k_{15g}[CO_2])} \quad \text{(A38)}$$

Manuscript received Nov. 16, 2009, and revision received Dec. 25, 2010.